THE ASTROPHYSICAL JOURNAL, 377:L21–L24, 1991 August 10

FIRST RESULTS FROM THE GODDARD HIGH-RESOLUTION SPECTROGRAPH: THE GALACTIC HALO AND THE Lyα FOREST AT LOW REDSHIFT IN 3C 273[1]

SIMON L. MORRIS AND RAY J. WEYMANN
Observatories of the Carnegie Institution of Washington, 813 Santa Barbara Street, Pasadena, CA 91101
BLAIR D. SAVAGE
University of Wisconsin, Department of Astronomy, 475 North Charter Street, Madison, WI 53706
AND
RONALD L. GILLILAND
Space Telescope Science Institute, 3700 San Martin Drive, Baltimore, MD 21218
Received 1991 March 28; accepted 1991 April 19

ABSTRACT

We present results of initial spectroscopy using the Goddard High-Resolution Spectrograph and the *Hubble Space Telescope* on the bright low-redshift quasar 3C 273. We detect absorption lines produced by gas in the disk and halo of the Milky Way from numerous neutral and weakly ionized atoms and also from highly ionized atoms (Si IV, C IV, and N V). The detection of N V provides additional strong support for the existence of gas with $T \sim 2 \times 10^5$ K at large distances away from the disk of the Milky Way. We also find 10 absorption lines with EW greater than 50 mÅ, and four possible lines with EW between 25 and 50 mÅ, in the region between 1235 and 1406 Å. These cannot be identified with any lines in the galactic interstellar medium and must therefore all be Lyα systems at very low redshifts. This number of lines is 5–10 times larger than expected from a simple extrapolation of the high-redshift evolution derived from ground-based observations and is consistent with no evolution in cloud properties since $z = 2$.

Subject headings: cosmology — interstellar: matter — quasars — ultraviolet: spectra

1. INTRODUCTION

The quasar 3C273 is the brightest AGN of any significant redshift in the sky and therefore is ideal for study of gas at large distances from the Galactic plane, and of Lyα absorption lines at low redshift. In this paper we describe observations taken with the Goddard High-Resolution Spectrograph (GHRS) on the *Hubble Space Telescope*, discuss the many absorption lines caused by gas in our Galactic halo and investigate the set of absorption lines from low-redshift Lyα clouds. Observations of 3C273 have also been obtained with the FOS and are described elsewhere in this issue (Bahcall et al. 1991 and Beaver et al. 1991), but the results reported here are based exclusively on the GHRS data.

2. OBSERVATIONS AND REDUCTIONS

Observations were made on 1991 February 23 (UT) consisting of a 980 s. G140L exposure covering 1175–1452 Å, six overlapping G160M exposures covering 1235–1425 Å, and G160M, G200M, and two G270M exposures covering 1522–1556, 1775–1813, 2572–2617, and 2777–2821 Å with exposure times ranging from 980 to 2940 s. The S/N per substepped pixel was 30 for the G140L exposure and averaged 9.0 for the G160M exposures. The Large Science Aperture (LSA) (2.″0 × 2.″0) was chosen rather than the SSA (0.″25 × 0.″25) because, at the time the aperture had to be specified, there were considerable uncertainties in acquisition and guiding. The point spread function thus consisted of a fairly sharp core, together with broad wings truncated by the edge of the LSA. The full width at half-maximum of the core corresponds to ~200 km s^{-1} for G140L and 20 km s^{-1} for the other exposures, while the wings extend to about ±700 and ±70 km s^{-1}, respectively.

The object was acquired using the onboard GHRS acquisition software. Wavelength calibration exposures were only taken whenever there was a grating change. Observations of the target were taken with GHRS substep pattern 5, which moves the spectrum on the diode array by steps of one-fourth of a diode. Approximately 6% of the time is spent measuring the (internal) background count rate. We also used the GHRS FP-SPLIT option, breaking each exposure into four parts between which the grating is moved by ~5 diodes, partially averaging out photocathode granularity. The separate FP-SPLIT exposures were also useful for identifying a few ion events which introduce non-Poissonian noise, but no attempt was made to remove them. The data were reduced using the IDL-based GHRS team software. Science Verification for the GHRS is still in progress so the wavelengths are preliminary, but we estimate that they are accurate to better than 1 diode, or ~0.6 Å for G140L and ~0.07 Å for G160M. The absolute flux calibration is probably good to ~10% for G140L, but is less well known for the other exposures. The geocoronal emission filling in Galactic Lyα absorption was subtracted using a scaled version of blank sky data taken from the failed SAO 3024 observation. No correction was made for geocoronal line emission from O I λ1302.

3. SPECTRA, DECONVOLUTION, LINE IDENTIFICATION, AND PROFILE FITTING

Figures 1*a* and 1*b* show, respectively, the spectra obtained with G140L and the shortest wavelength G160M exposure. The remaining exposures will be published elsewhere (Brandt et al. 1991). We have also plotted the 1 σ errors. Note that although the S/N per substep pixel in the G160M data is low,

[1] Based on observations with the NASA/ESA *HST*, obtained at the STScI, which is operated by AURA, Inc., under NASA contract NAS5-26555.

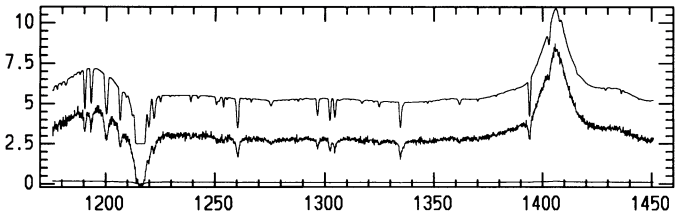

FIG. 1*a*

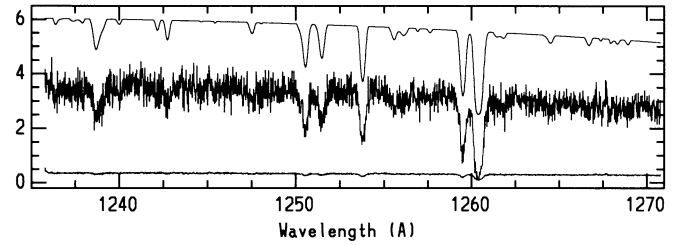

FIG. 1*b*

FIG. 1.—(*a*) 3C 273 GHRS G140L exposure, raw data with 1 σ error and deconvolution of data using the Jansson (1984) technique imposing bounds at zero and the assumed continuum level. The *y*-axis is F_λ in units of 10^{-13} ergs cm^{-2} s^{-1} $Å^{-1}$, with the deconvolved spectrum shifted upward by 2.5×10^{-13}. (*b*) The bluest G160M exposure. For most of the absorption lines, the raw data is highly oversampled. Convolved data were prefiltered, resulting in significant smoothing associated with the deconvolution.

the data is significantly oversampled, and considerable smoothing is possible without loss of information.

In an attempt to recover some of the resolution lost because of the use of the LSA we have applied deconvolution techniques to the data, exploring two approaches: (1) deconvolution in the Fourier domain (see Press et al. 1986) and (2) a nonlinear iterative technique (Jansson 1984) that allows imposition of bounds, e.g., positivity, and an upper bound at an assumed continuum level. The Jansson technique can produce superior results where such constraints are important. The spectra deconvolved with the Jansson technique are also shown in Figures 1*a*–1*b*. A detailed discussion of these techniques will be presented elsewhere (Gilliland et al. 1991).

Three separate searches for absorption features were made. Two of us (S. L. M., R. J. W.) independently examined the data for absorption features, measured the wavelengths and equivalent width (EW) using the IRAF SPLOT task, and classified the lines into "certain" and "possible" features. The raw spectra were also passed through an automatic line finding algorithm, part of an analysis package developed by R. F. Carswell and J. K. Webb, and kindly made available to us. For each line, the algorithm yields a wavelength, EW, and the probability that this EW would not be exceeded by Poisson fluctuations. Good agreement was found from these three searches. The observed (vacuum, heliocentric-corrected) wavelengths are given in column (1) of Table 1. Column (2) contains the measured EW. The values quoted are means from the three searches. Column (3) is minus the log of the probability for the line *not* being real, as calculated by the algorithm. Based on the RMS of the measurements from the three searches, we estimate that the typical 1 σ error for our EW from the intermediate resolution data is 10 mÅ. For the lines seen only in the G140L data the error is more uncertain, but we estimate a 1 σ error of

TABLE 1

LINE LIST

λ_{obs} (Å) (1)	EW_{obs} (mÅ) (2)	−log (*P*) (3)	Ion (4)	Velocity *z* (5)	*b* (6)	log *N* (cm^2) (7)	
1190.5.....	426	L	Si II	...	...	...	
1193.5.....	389	L	Si II	...	...	...	
1200.4.....	713	L	N I	...	...	...	
1206.8.....	445	L	Si III	...	...	...	
1215.....	7800:	L	H I	...	...	...	
1220.0.....	...	L	H I	0.0036	...	...	a
1222.2.....	...	L	H I	0.0057	...	...	a
1238.75....	145	>7.5	N V	−17	...	13.90	b
1242.17....	27	6.0	H I	0.02180	23	12.87	c
1242.72....	52	>7.5	N V	−20	...	...	b
1247.54....	32	5.2	H I	0.02622	49	13.01	
1250.53....	164	>7.5	S II	−4	...	...	b
1251.46....	120	>7.5	H I	0.02944	36	13.48	
1253.78....	183	>7.5	S II	−7	...	...	b
1255.70....	74	>7.5	H I	0.03293	111	13.30	
1259.50....	274	>7.5	S II	−5	...	...	b
1260.40....	590	>7.5	Si II	−5	...	...	b
1275.19....	144	>7.5	H I	0.04896	24	13.55	
1276.54....	68	>7.5	H I	0.05007	17	13.04	
1289.79....	52	5.9	H I	0.06097	63	13.06	
1292.84....	63	>7.5	H I	0.06348	34	13.12	
1296.57....	302	>7.5	H I	0.06655	28	14.13	
1302.07....	415	>7.5	O I	−23	...	...	
1304.29....	385	>7.5	Si II	−18	...	...	b
1322.16....	75	>7.5	H I	0.08760	56	13.23	
1324.96....	27	5.9	H I	0.08983	45	13.05	
1325.22....	57	>7.5	H I	0.09012	18	13.57	d
1334.49....	622	>7.5	C II	−9	...	...	
1335.72....	116	>7.5	C II*	4	...	...	
1361.63....	126	>7.5	H I	0.12007	20	13.52	
1370.09....	79	>7.5	Ni II	−9	...	...	e
1393.64....	367	>7.5	Si IV	−25	...	...	f
1393.86....	331	D	H I	0.14658	37	13.97	f
1402.65....	217	>7.5	Si IV	−26	...	13.78	f
1423.04....	43	>7.5	NoID	...	...	...	g
1526.66....	551	>7.5	Si II	−9	...	...	b
1534.71....	78	5.7	NoID	...	...	...	h
1548.16....	530	>7.5	C IV	−7	...	...	b,i
1550.72....	388	>7.5	C IV	−10	...	14.51	b,i
1807.98....	118:	>7.5	Si II	−5	...	...	b
2576.71....	197	>7.5	Mn II	−19	...	...	b
2586.46....	747	>7.5	Fe II	−22	...	...	
2589.98....	33	6.4	NoID	...	...	...	j
2594.27....	142	>7.5	Mn II	−26	...	...	b
2600.01....	942	>7.5	Fe II	−19	...	...	
2606.28....	90	>7.5	Mn II	−21	...	...	b
2796.31....	1167	>7.5	Mg II	−5	...	...	
2803.49....	1078	>7.5	Mg II	−4	...	...	

NOTES.—Probability code: L = only observed with G140L, D = not resolved by line finder. Velocity and *b* in km s^{-1}. Values followed by a colon are uncertain.

[a] On wing of damped Lyα; EW very uncertain.

[b] Voigt fit to all lines in given ion yield column densities of 13.98 (N V), 15.40 (S II), 14.75 (Si II), 13.83 (Si IV), 14.48 (C IV), and 13.16 (Mn II).

[c] Line did not improve χ^2 of fit to N V doublet.

[d] Fit parameters uncertain, depend on deblending.

[e] Second Ni II line at 1317.217 Å not detected in G160M data, but clearly seen in G140L exposure.

[f] Total EW of blend 566 mÅ; log *N*, *b* for Lyα from Voigt fit, and EW is expected value in absence of Si IV; *N*(Si IV) from integration over 1402 Å profile.

[g] Only "certain" line with no ID, but note it is not seen in G140L spectrum.

[h] Broad feature symptomatic of noise.

[i] Listed log *N* includes 0.09 dex correction for saturation as in Savage & Sembach 1991.

[j] Narrow feature symptomatic of noise.

$\sim$80 mÅ. Only lines with values of $-\log(P)$ from the algorithm exceeding 5.0 are listed. Henceforth we refer to lines with values exceeding 7.5 as "certain" and those having values between 5.0 and 7.5 as "possible." It must be stressed that the formal significance of these estimates depends sensitively on the placement of the continuum, and on the assumption that there are no significant non-Poissonian sources of noise. This latter point has not yet been adequately investigated for the GHRS. We have not tried to provide probability estimates for lines detected only with the G140L grating, due to the difficulty in continuum fitting shortward of 1220 Å, and these are simply designated with an "L" in column (3). The uncertainty in the subtraction of geocoronal Lyα over a range of $\sim$6 Å, together with the steep damping wings from Galactic Lyα makes the detection of lines from $\sim$1212 to 1220 Å especially difficult, though we believe the features at 1220.0 and 1222.2 Å to be real. Both of these features are readily visible in the deconvolved spectrum of Figure 1*a*.

Column (4) contains the identifications for all features which can be identified with galactic absorption. For these features, column (5) gives the velocity in the heliocentric rest system, using laboratory wavelengths given by Morton (1991). We have carefully searched Morton's line lists and examined intermediate resolution GHRS spectra of μ Columbae and HD 93521. We found no plausible Galactic identifications for the remaining 16 lines of Table 1 with wavelengths between the Galactic Lyα line and the peak of the Lyα emission line in 3C 273, nor can they be plausibly identified with metal lines having nonzero redshifts. *These lines must therefore all be* Lyα *lines with redshift between 0.0 and 0.156*. They are thus identified as such in column (4), while column (5) gives the computed redshift for these lines. Unfortunately, Lyβ lies shortward of our shortest observed wavelength for all but one of these lines, and on the extreme edge of the G140L exposure for that line (see § 4).

We have fitted the original (undeconvolved) profiles for all of the lines in Table 1 observed with the intermediate resolution gratings. We used a Voigt profile fitting algorithm which is also part of the Carswell-Webb package. This requires an estimate of the instrumental profile. We used a profile derived from the models of Burrows et al. (1991). An indication of the *internal* precision with which the column density and Doppler parameter (b) can be determined is provided by the line at 1361.6 Å, which appears on two different exposures. For this line the two log N and b values differ by 0.05 and 1.5 km s^{-1}, respectively. The values of the column density and b for the Lyα lines are listed in columns (6) and (7). Due to the large uncertainties in the fits to the halo lines we only give the derived column densities as notes to Table 1. For the halo lines of N v, Si iv, and C iv, column densities were also estimated by a direct integration over the profiles (see § 4). These values are given in column (7).

4. GALACTIC ABSORPTION FEATURES

Absorption lines from gas in the disk and halo of the Milky Way have been detected from the following species: H i, O i, C ii, C ii*, C iv, N i, N v, Si ii, Si iii, Si iv, S ii, Mg ii, Mn ii, Fe ii and Ni ii. H i 21 cm emission measurements toward 3C 273 ($l = 290°$, $b = 65°$) obtained with the NRAO 140 foot (43 m) telescope (Lockman & Savage 1991), reveal strong H i emission centered near $v_{\rm helio} \sim -11$ km s^{-1} with extensions to -58 km s^{-1} and $+42$ km s^{-1} and no evidence for high-velocity H i between -270 and $+170$ km s^{-1}. Our estimate for the H i column density from the (very uncertain) fit to the damping wings of the Galactic Lyα is $10^{20.1\pm0.2}$ cm^{-2}, consistent with the value $10^{20.23\pm0.015}$ cm^{-2}, obtained from the 21 cm emission measurement. The extent of the H i emission implies that large f-value UV lines of abundant elements would be expected to be optically thick over $\sim$100 km s^{-1}, as appears to be the case. For example, the strongest lines of O i, C ii, Si ii, and Mg ii have full widths at half-intensity ranging from 110 (O i) to 145 km s^{-1} (C ii and Si ii). The strong lines are apparently sampling the low column density, high velocity dispersion gas seen in the 21 cm emission profile. Neutral and weakly ionized gas populating the low halo may contribute to absorption in these lines.

The absorption by N v, C iv and Si iv is also very strong. Because the line profiles for the highly ionized gas are broad and asymmetric, we did not rely on Voigt profile fitting, but also estimated column densities by direct integration over the profiles for Si iv λ1402, C iv $\lambda\lambda$1550 and 1548 and N v λ1238. These column densities, listed in Table 1, are $\sim$2 times larger than those found for the gas associated with the Milky Way (with $v < 120$ km s^{-1}) for the sight line to the SMC ($l = 302°$, $b = -45°$) and are consistent with the trends established by the survey of highly ionized gas in the galactic halo (Savage & Massa 1987).

The detection of N v is quite significant because it is a diagnostic of gas with $T \sim 2 \times 10^5$ K, which cools very rapidly. Its origin may be associated with the cooling gas of a Galactic fountain (Shapiro & Field 1976; Edgar & Chevalier 1986) or with thermal condensations in cosmic-ray–driven fountains (Hartquist & Morfill 1986), and its detection provides additional strong support for the existence of hot gas extending away from the disk as first described by Spitzer (1956).

The Si iv $\lambda\lambda$1393 and 1402 lines reveal a problem: their EWs differ by more than a factor of 2, and the mean velocity of λ1393 line is anomalous. Nevertheless, the Si iv GHRS data are in approximate agreement with the *IUE* observations (York et al. 1983) and the GHRS G140L deconvolved results also indicate an EW ratio greater than 2. We believe that Si iv λ1393 is contaminated with another line, and we have estimated the required properties of that line in two ways: (1) We used the Voigt profile algorithm to fit the two Si iv lines, including an additional component in the λ1393 complex. (2) From the Si iv λ1402 line we derived the optical depth as a function of velocity, computed from this the expected absorption associated with Si iv λ1393, and from the observed λ1393 profile inferred the properties of the additional absorber. The two results agree quite well and require a strong line situated at about $+50$ km s^{-1} with respect to Si iv λ1393. As in the case of the other unidentified lines shortward of the Lyα emission, we assume that this line is Lyα, but consider it as "possible" rather than "certain" despite its large derived EW. The corresponding Lyβ line should lie on the blue edge of our G140L exposure at 1176.07 Å with an EW of 71 mÅ. No such line is seen, but our 3 σ upper limit there is only $\leq$120 mÅ.

5. Lyα FOREST AT ZERO REDSHIFT

Before the launch of HST, essentially nothing was known about the Lyα forest below redshifts of 1.6 (see Hunstead 1988 and Carswell 1988 for recent reviews of the high-redshift Lyα forest). Our discovery of at least nine and possibly 16 very low redshift lines of Lyα leaves little doubt that the Lyα lines persist to zero redshift.

Our weakest "possible" line has a *rest* EW of 25 mÅ while, aside from the line blended with Si iv λ1393, the strongest has an EW of 49 mÅ. The weakest "certain" line has an EW of 52

mÅ. For the rest of this discussion we therefore adopt 25 and 50 mÅ as the thresholds for "weak" and "strong" lines. We will *not* include the lines at 1220.0 and 1222.2 Å in our analysis below, as the EW limit for the G140L data is uncertain, and differs from that of the G160M data. We thus have EW–limited samples of 10 "strong" and 4 "weak" Lyα absorption lines between redshifts of 0.016 and 0.156. (Our S/N varies only slightly over this range.) Because of the "proximity effect," (see Bajtlik, Duncan, & Ostriker 1988) we exclude the redshift region 0.151–0.156 over which photoionization from 3C 273 exceeds that from the UV background (Songaila, Bryant, & Cowie 1989).

If we assume that the distribution of Lyα lines as a function of redshift and EW has the form and parameters derived at high redshift (as in Murdoch et al. 1986), then over the redshift range of 0.016–0.151 one predicts 0.8–2.1 lines with rest EW greater than 50 mÅ, whereas we observed 10. One predicts 0.9–2.3 lines with rest EW greater than 25 mÅ, whereas we have possibly observed 14. The range given in predicted number of clouds corresponds to the 1 σ error range in the input parameters. Thus it appears that the high-redshift parameterization significantly underestimates the number of Lyα lines at very low redshift. (Note that the conclusions of Murdoch et al. [1986] refer to a much stronger EW domain.)

To see whether this underestimate arises mainly because of a change in the EW distribution with redshift, we compare our low-redshift EW distribution with that at high redshift, using the data of Carswell et al. (1991) and Pettini et al. (1990). We adopt a limiting rest EW of 50 mÅ to which all three samples seem complete. A two-sided KS test gives no statistically significant indication of a difference in the EW distribution of the low and high-redshift samples. With this conclusion, we can then calculate the best value for γ, $[\partial N/\partial z \propto (1+z)^{\gamma}]$, following the maximum likelihood estimation procedure of Murdoch et al. (1986) and using our data combined with that of Carswell et al. (1991). We obtain a γ of 0.79 with 1 σ error of ± 0.37, a value very much lower than the value of 2.36 ± 0.40 found for the high-redshift regime (see Bajtlik, Duncan, & Ostriker 1988). *This suggests that there is a significant decrease in the rate at which the Lyα forest thins out, occurring at some redshift less than* ~ 2. The value of γ we derive between $z = 2$ and $z = 0$ is consistent with a constant number of clouds of given column density and cross section per co-moving volume element, for q_0 between 0 and $\frac{1}{2}$. A K-S test also shows no evidence for a nonuniform redshift distribution over the very small redshift range (0.016–0.151) of our sample.

It is difficult to be certain that these low-redshift systems represent the same phenomenon as the high-redshift ones. Two characteristics of the high-redshift Lyα forest lines are noteworthy: (1) For Lyα lines with column densities less than $\sim 10^{16}$ cm^{-2} there are no associated metal lines (see, e.g., Chaffee et al. 1985) and attempts to detect metal line counterparts to the weaker Lyα forest lines by co-adding a large number of spectra only give upper limits to the column density ratios (Williger et al. 1989, but also see Lu 1991). (2) There is no measurable clustering of the Lyα forest lines (Sargent et al. 1980), except perhaps at extremely small velocity separations (Barcons & Webb 1990). The existing data on 3C 273 are not adequate for meaningful limits to be set by the co-addition technique on the column density ratio of C IV/Lyα or C II/Lyα. However, we note that at the redshift of our strongest Lyα line at 1296.57 Å, C II λ1334.53 should appear ~ 63 km s^{-1} to the red of the unidentified line at 1423.04 Å. We think this identification unlikely, but it can be decisively tested by a relatively short G270M exposure at the expected position of the Mg II doublet at ~ 2985 Å. We have performed a clustering analysis on the set of 14 "possible + certain" lines found in the G160M exposures and find no convincing evidence for clustering at any scale, but the sample size must be increased before this test becomes a critical one. In summary, we can only say that our data are consistent with the low-redshift Lyα lines having the same basic properties as the high-redshift Lyα forest.

Despite their proximity, (the lines at 1220.0 and 1222.2 Å may arise from clouds within the Virgo cluster), we note that attempts to image these low column density clouds in either recombination radiation (Lyα or Hα) or 21 cm emission seem unlikely to succeed without an increase in sensitivity of several orders of magnitude. Whatever their nature, we consider it remarkable that such tenuous entities have managed to survive or have been continuously regenerated over a Hubble time.

We thank Dennis Ebbets, Eliot Malumuth, and Cindy Peck for assistance during the observations, Dara Norman, Ulysses Sofia, and Laura Ferrarese for assistance in reducing the data, Bob Carswell and John Webb for allowing use of their line analysis software, and Bob Carswell for copious advice on its use. Special thanks go to Jack Brandt and Sally Heap for their tireless efforts on behalf of the GHRS team. S. L. M. and R. J. W. acknowledge support through NASA contract NAS5-30101 and NSF grant AST 90-05117. B. D. S. acknowledges support through NASA contract NAS5-29638.

REFERENCES

Bahcall, J., et al. 1991, ApJ, 377, L5
Bajtlik, S., Duncan, R. C., & Ostriker, J. P. 1988, ApJ, 327, 570
Barcons, X., & Webb, J. K. 1990, MNRAS, 244, 30P
Beaver, E. A., et al. 1991, in preparation
Brandt, J. C., et al. 1991, in preparation
Burrows, C. J., Holtzman, J. A., Faber, S. M., Bely, P. Y., Hasan, H., Lynds, C. R., & Schroeder, D. 1991, ApJ, 369, L21
Carswell, R. F. 1988, in STScI Symp. Ser. 2, QSO Absorption Lines: Probing the Universe, ed. C. J. Blades, D. Turnshek & C. A. Norman (Cambridge: Cambridge University Press), 91
Carswell, R. F., Lanzetta, K. M., Parnell, H. C., & Webb, J. K. 1991, ApJ, 371, 36
Chaffee, F. H., Foltz, C. B., Roser, H. J., Weymann, R. J., & Latham, D. W. 1985, ApJ, 292, 362
Edgar, R. J., & Chevalier, R. A. 1986, ApJ, 310, L27
Gilliland, R. L., et al. 1991, in preparation
Hartquist, T. W., & Morfill, G. E. 1986, ApJ, 311, 518
Hunstead, R. W. 1988, in STScI Symp. Ser. 2, QSO Absorption Lines: Probing the Universe, ed. C. J. Blades, D. Turnshek & C. A. Norman (Cambridge: Cambridge University Press), 71
Jansson, P. A. 1984, Deconvolution: with Applications in Spectroscopy (New York: Academic)
Lockman, F. J., & Savage, B. D. 1991, in preparation
Lu, L. 1991, preprint
Morton, D. C. 1991, ApJS, in press
Murdoch, H. S., Hunstead, R. W., Pettini, M., & Blades, J. C. 1986, ApJ, 309, 19
Pettini, M., Hunstead, R. W., Smith, L., & Mar, D. P. 1990, MNRAS, 246, 545
Press, W. H., Flannery, B. P., Teukolsky, S. A., & Vetterling, W. T. 1986, Numerical Recipes (Cambridge: Cambridge University Press)
Sargent, W. L. W., Young, P. J., Boksenberg, A., & Tytler, D. 1980, ApJS, 42, 41
Savage, B. D., & Massa, D. 1987, ApJ, 314, 38
Savage, B. D., & Sembach, K. 1991, ApJS, submitted
Shapiro, P. R., & Field, G. B. 1976, ApJ, 205, 762
Songaila, A., Bryant, W., & Cowie, L. L. 1989, ApJ, 345, L71
Spitzer, L. 1956, ApJ, 124, 20
Williger, G. M., Carswell, R. F., Webb, J. K., Boksenberg, A., & Smith, M. G. 1989, MNRAS, 237, 635
York, D. G., Wu, C. C., Ratcliff, S., Blades, J. C., Cowie, L. L., & Morton, D. C. 1983, ApJ, 274, 136